

Investigation of a laser-produced cerium plasma by the analysis of the high-resolution x-ray spectrum

R. Doron, E. Behar, M. Fraenkel, P. Mandelbaum, J. L. Schwob, and A. Zigler
Racah Institute of Physics, The Hebrew University, 91904 Jerusalem, Israel

A. Ya. Faenov and T. A. Pikuz

Multicharged Ion Spectra Data Center, VNIIFTRI, Mendel'ëvo, Moscow Region, 141570 Russia

(Received 12 January 2000; revised manuscript received 8 May 2000; published 13 October 2000)

A highly stripped cerium ($Z=58$) plasma is produced by irradiating a solid cerium target with a short pulse laser. The x-ray spectrum emitted from the plasma is recorded in the limited wavelength range 9.0–9.3 Å using a high-resolution curved mica crystal spectrometer. The high-resolution spectrum, which corresponds to the $3d$ - $5f$ transitions in Ni-, Cu-, and Zn-like cerium ions, is analyzed by means of a detailed collisional-radiative model that includes autoionization and dielectronic capture processes. The intensity ratio of the Ni-like $3d$ - $5f$ resonant line at 9.045 Å to the features emitted from satellite transitions of Cu-like ions provides an estimate for the mean electron temperature and density of 230 eV and 10^{22} cm $^{-3}$, respectively. The deduced mean electron temperature is higher than that obtained in a similar experiment on laser-produced barium plasma. The origin of the higher mean electron temperature deduced in the present experiment is explained by the different type of transition employed for the temperature diagnostics, which might reflect a different phase of the plasma evolution.

PACS number(s): 32.30.Rj, 32.70.-n, 52.70.-m

I. INTRODUCTION

Plasmas of highly ionized heavy elements are now routinely produced by compact high-power lasers in a large number of laboratories. The emission of these plasmas can be used as a bright source of x-ray radiation in the 1-keV energy range. Another area of interest associated with the emitted spectra is the role that transitions in which doubly (or inner-shell) excited autoionizing configurations are involved can play in the ionization balance in highly ionized plasmas. Of particular interest are the $3d$ - nf ($n \geq 4$) transitions in ionization states lower than the Ni I isoelectronic sequence (e.g., $3d^{10}nl$ - $3d^9n14f$ in Cu-like ions), which have been found to be important channels for excitation autoionization [1], as well as for stabilization following dielectronic capture processes [2]. In turn, the emission from these transitions can be useful for plasma diagnostic purposes.

The x-ray spectrum in the spectral range of 10–12 Å emitted from a cerium ($Z=58$) plasma has already been observed with low spectral resolution using a vacuum high-power spark [3]. In that work, the $3p$ - $4d$, $3d$ - $4f$, and $3p$ - $4s$ transitions of Ni-like Ce ions were identified, and their intensities were used to estimate the electron density of the prepinched phase of the cerium spark plasma. In a recent work, a much more comprehensive detailed identification of the x-ray spectrum in the wavelength range 7.5–12 Å emitted from a laser-produced cerium plasma and recorded with a flat crystal spectrometer was presented [4]. The work was the continuation of similar spectroscopic investigations carried out for analyzing the x-ray spectra in the 1-keV energy range emitted from lanthanum ($Z=57$), praseodymium ($Z=59$) [5], and barium ($Z=56$) [6] laser-produced plasmas. Most of the unresolved transition array (UTA) features appearing in these spectra arise from transitions in which doubly excited

configuration complexes are involved. For ionization states lower than Ni I, these features correspond to transitions of the type $3d^{10}4l^x$ - $3d^94l^xnf$ ($n \geq 4$, $x=1$ for Cu-like ions, $x=2$ for Zn-like ions, etc.). It is well known by now that, under the typical conditions prevalent in laser-produced plasmas, transitions involving $4l$ electron spectators with *all* possible l values do contribute to the *detailed* structure of the observed UTA features. Such detailed components of the spectrum were first observed for high- Z ions in the high-spectral-resolution barium spectrum, recorded in the range 9.0–9.3 Å using a curved mica crystal spectrometer [7]. The emission in this spectral range corresponds to the $3d$ - $6f$ transitions of Cu- and Zn-like barium ions, in which all of the upper doubly excited configurations are autoionizing. This high-resolution spectrum was interpreted by employing a detailed collisional-radiative model that takes autoionization and dielectronic recombination processes into account. The results of the model enabled an estimate of the electron density and temperature, and indicated that the observed transitions can be attributed mostly to dielectronic capture processes that probably take place during the cooling phase of the plasma [7].

In the present work, a similar experimental setup to the one described in Ref. [7] is used in order to record the x-ray spectrum emitted from a highly stripped cerium ($Z=58$) plasma. The spectrum is recorded in the limited wavelength range 9.0–9.3 Å using a very high-resolution spherically bent mica crystal spectrometer [8], in parallel to the observation of the whole wavelength range 7.5–12 Å using a low-resolution flat rubidium acid phthalate (RAP) crystal. While the lower-resolution spectrum exhibits mostly unresolved transition array features of Ni-like and neighboring ionization states [4], the high-resolution spectrum, which corresponds to $3d$ - $5f$ transitions in Ni-, Cu-, and Zn-like cerium, reveals many additional detailed features. In contrast to the

high-resolution barium spectrum [7], the present high-resolution cerium spectrum includes not only Cu- and Zn-like dielectronic satellites, but also a Ni-like resonant transition. This Ni-like line cannot originate from dielectronic capture processes but rather must come from electron impact excitations, and therefore the diagnostic based on this radiation might reflect a different phase of the plasma evolution.

II. EXPERIMENT

The plasma is created by irradiation of solid cerium targets by intense ultrashort laser pulses. The laser generates 25-mJ, 120-fs pulses at a repetition rate of 10 Hz. The power ratio between the prepulse and the main pulse is about 10^{-3} . The laser is based on a Ti:sapphire oscillator generating 80-fs pulses at a wavelength of 800 nm with a spectral width of about 10 nm. The 80-fs pulse is amplified by the chirped pulse amplification technique [9] in which it is first stretched temporarily to a width of about 1 ns. Subsequently, it is sent into a regenerative amplifier and a four-pass amplifier, and finally it is recompressed to a pulse width of 120 fs. The laser pulse is focused on the Ce target to a focal spot of about 20- μ m diameter, producing a laser power density of 6×10^{16} W/cm².

The x rays emitted by the plasma are dispersed by a high-resolution ($\lambda/\Delta\lambda \sim 8000$) spherical mica crystal [8], and the spectrum is recorded on Kodak Direct Exposure film shielded by a visible-light absorber. The positions of the spectral lines on the photographic films are measured both by means of a Grant comparator and also by digitally scanning the films using a high-optical-density and high-resolution charge-coupled device. The Grant comparator has a higher spatial resolution, whereas the scanner gives more reliable line intensities. Only spectra recorded by the scanner are shown in this paper. The accuracy of the wavelength measurements performed using the mica crystal is estimated to be better than 1 mÅ, based on recent high-resolution measurements of He- and Li-like magnesium reference lines [10]. The radiation emitted by the plasma is simultaneously dispersed by a flat RAP crystal for which the absolute intensities can be derived by introducing accurate corrections to account for the film sensitivity [11], the RAP crystal reflectivity [12], the visible-light filter transmission, and the source-to-film distance.

III. THEORETICAL METHOD

In order to exploit the additional information provided by the high-resolution spectrum, it is essential to construct a detailed model that includes configurations with high- l value electron spectators. In two recent works [7,13], a level-by-level two-step collisional-radiative model was developed and employed for simulating the spectra emitted from autoionizing levels. In the present work, this detailed model is used to reproduce theoretically the high-resolution cerium spectrum in the wavelength range 9.0–9.3 Å, which is identified as originating mainly from $3d-5f$ transitions of Ni-, Cu-, and Zn-like Ce ions. Since the details of the model have already been presented [7,13], only a brief description is given here.

Each pair of adjacent ionization states (i.e., Co I and Ni I, Ni I and Cu I, and Cu I and Zn I) is considered separately in the model. In a first step, the populations of the *ground* or *singly excited* levels of the recombining ion (e.g., Ni I), denoted n_k , and those of the emitting ion (e.g., Cu I), denoted n_i , are calculated by solving two separate sets of collisional-radiative rate equations.

In the second step, the populations of the *doubly* (or inner-shell) *excited* levels d of the emitting ion are calculated. For the doubly excited levels the following atomic processes are included: radiative decays to lower doubly excited levels and collisional transitions between the doubly excited levels d and d' , radiative decays to the ground and singly excited levels, collisional excitations and deexcitations from and to the ground and singly excited levels, autoionization, dielectronic capture, collisional ionization, and three-body recombination. Radiative recombination is neglected. The steady-state collisional-radiative set of rate equations for the levels d can be written as follows:

$$\begin{aligned} \frac{dn_d}{dt} = & n_e \sum_{d' \neq d} n_{d'} Q_{d'd}(T_e) + \sum_{d' > d} n_{d'} A_{d'd} \\ & - n_d \left[n_e \sum_{d' \neq d} Q_{dd'}(T_e) + \sum_{d' < d} A_{dd'} \right] \\ & + n_e \left[\sum_i n_i Q_{id}(T_e) + \sum_k n_k \beta_{kd}^c(T_e) \right. \\ & \left. + n_e \sum_k n_k \beta_{kd}^{\text{TB}}(T_e) \right] - n_d \left[n_e \sum_i Q_{di}(T_e) + \sum_k A_{dk}^a \right. \\ & \left. + n_e \sum_k S_{dk}(T_e) + \sum_i A_{di} \right] = 0. \end{aligned} \quad (1)$$

T_e is the electron temperature. $Q_{d'd}(T_e)$ denotes the rate coefficient for collisional excitation or deexcitation from level d' to level d , and $A_{d'd}$ is the Einstein coefficient for radiative decay from d' to d . $\beta_{kd}^c(T_e)$ is the rate coefficient for dielectronic capture from k to d , and A_{dk}^a is the rate for the reverse process, i.e., autoionization from d to k . $\beta_{kd}^{\text{TB}}(T_e)$ is the rate coefficient for three-body recombination from k to d , and $S_{dk}(T_e)$ the rate coefficient for the reverse process, i.e., collisional ionization from d to k . The densities n_i and n_k are taken from the results of the first-step procedure. Radiation trapping effects are included in the model by correcting the Einstein coefficients using the mean escape factor approximation developed by Breton and Schwob [14] (described also in Ref. [13]). Finally, the level population n_d calculated in the model together with the computed Einstein coefficients for radiative decays are used to create the simulated spectrum.

All the atomic quantities needed for the model (level energies, spontaneous emission and autoionization coefficients, and cross sections for all the inelastic collisional processes) are generated by *ab initio* relativistic calculations using the HULLAC (Hebrew University Lawrence Livermore atomic code) computer package [15].

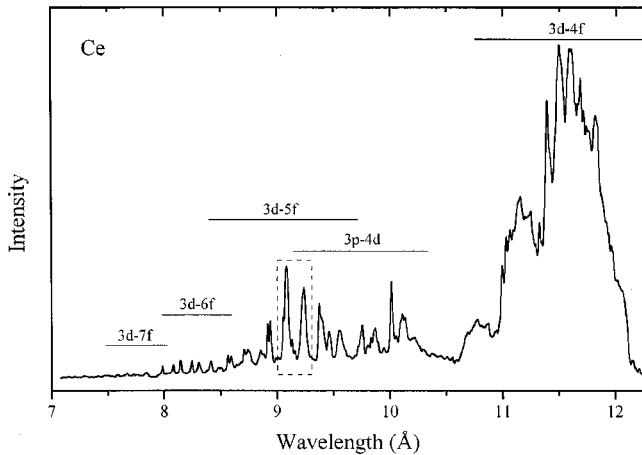


FIG. 1. X-ray spectrum of the laser-produced cerium plasma obtained in the wavelength range 7.5–12 Å using the flat RAP crystal. The ranges of the transitions between configurations belonging to the Ni-like and neighboring ionization states are indicated above the spectrum. The dashed rectangle in the 3d-5f range shows the spectral region recorded with a higher resolution using the spherical mica crystal.

IV. IDENTIFICATION OF INDIVIDUAL LINES

Figure 1 shows the experimental cerium spectrum recorded in the whole wavelength range 7.5–12 Å, using the low-resolution flat RAP crystal spectrometer. The ranges of the transitions between configurations identified in the previous work [4] as belonging to the Ni-like and neighboring ionization states are indicated above the experimental spectrum. The limited wavelength range 9.0–9.3 Å in which the high-resolution spectrum investigated in the present work was obtained is indicated by the dashed rectangle. This limited spectral range is shown in detail in Fig. 2, where the high-resolution spectrum obtained using the spherical mica crystal [Fig. 2(a), thick trace] is compared to the spectrum obtained by means of the flat RAP crystal [Fig. 2(b)] recorded in the same wavelength range. The main spectral features observed, as previously identified in Ref. [4], are the 3d-5f transitions of Ni-, Cu-, and Zn-like cerium. The weaker feature of the 3s-4p_{1/2} transition of Ni-like Ce³⁰⁺ is observed as well, and also possibly the 3p-4d transitions of Co-like Ce³¹⁺. These identifications are reported above the lower-resolution spectrum in Fig. 2(b).

The line wavelengths and intensities of the high-resolution spectrum are analyzed using the collisional-radiative model described in Sec. III. The doubly excited configurations that are the upper levels of the main radiative transitions observed in the high-resolution spectrum and that have been included in the model are 3dⁿl5f ($n=4,5$) for the Cu-like ion and 3d⁹4s4l5f for the Zn-like ion. Where the computational limitations allow, other close-lying configurations that mix strongly with the above configurations were concluded as well. In order to improve the predictions of the model, the most important radiative decays to lower doubly excited configurations, for example, 3d⁹4l4l' in the Cu-like case, are also taken into account. For the Ni-like ion the following configurations are included in the model:

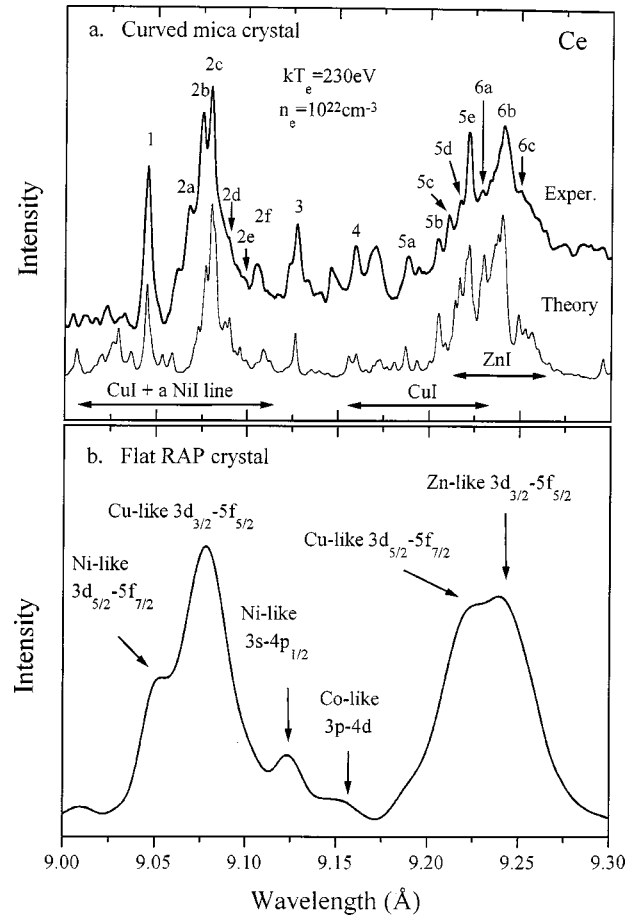


FIG. 2. X-ray spectrum of laser-produced cerium plasma in the wavelength range 9.0–9.3 Å. The thick trace in (a) is a recording of the spectrum obtained with the high-resolution spherical mica crystal spectrometer compared to the synthetic spectrum (thin curve) calculated for $n_e = 10^{22} \text{ cm}^{-3}$ and $kT_e = 230 \text{ eV}$. (The 3p-4d Co-like transitions were not modeled.) Labels containing a letter correspond to the transition identifications in Table I. The trace in (b) is the recording obtained with the flat RAP crystal. The UTA identifications as reported in Ref. [4] are given above the spectrum (b).

$3s^2 3p^6 3d^{10}$, $3s 3p^6 3d^{10} 4l$, $3s^2 3p^5 3d^{10} 4l$, and $3s^2 3p^6 3d^9 n l$ ($n=4,5,6$). The total number of levels included in the model are 255 for the Ni-like ion, 1753 for the Cu-like ion, and 2434 for the Zn-like ion. Since in the following analysis we focus on the emission from the Ni-, Cu-, and Zn-like ions, the 3p-4d transitions of Co-like cerium are not modeled in the present work. This explains some of the missing lines in the theoretical spectrum in Fig. 2(a) (namely, in the range 9.14–9.20 Å).

In Fig. 2(a), the synthetic spectrum (thin trace) obtained by modeling the Ni-, Cu-, and Zn-like line wavelengths and intensities is compared to the high-resolution experimental spectrum. In order to further improve the agreement with experiment and to make easier the comparison of the detailed structures due to weak lines and complete the line identification, the theoretical wavelengths of the lines in Fig. 2(a) have been shifted by very small amounts. The theoretical wavelengths of all the lines composing the complex spectral structures belonging to the Cu- and Zn-like ionization states

TABLE I. Experimental and theoretical line wavelengths of the high-resolution cerium spectrum in the range 9.0–9.3 Å and the corresponding $3d$ - $5f$ transitions identified in the Ni-, Cu-, and Zn-like cerium ions. Labels refer to the peaks of the experimental spectrum in Fig. 2(a). Only theoretical wavelengths of the strongest lines that contribute to each identified peak are given. gA is the calculated Einstein coefficient for spontaneous emission multiplied by the upper-level statistical weight. $X[Y]$ stands for $X \times 10^Y$. For the upper level of each transition, the most important components of the eigenvector are given, preceded by the square of their coefficients. J_L and J_U are the total angular momenta of the lower and upper levels, respectively.

Label	λ_{expt} (Å)	Ion	Sequence	λ_{theor} (Å)	gA (s^{-1})	Line transition	J_L	J_U
1	9.0450	Ce ³⁰⁺	Ni I	9.064	4.2[13]	$3d^{10}$ 80% $3d_{5/2}^9 5f_{7/2}$	0	1
2a	9.0676	Ce ²⁹⁺	Cu I ^a	9.064	2.0[14]	$3d^{10}4p$ 44% $(3d_{3/2}^9 4p_{3/2})_2 5f_{5/2}$ + 28% $(3d_{3/2}^9 4p_{3/2})_1 5f_{5/2}$	3/2	5/2
2b	9.0747	Ce ²⁹⁺	Cu I	9.066	1.4[14]	$3d^{10}4d$ 68% $(3d_{3/2}^9 4d_{5/2})_4 5f_{5/2}$	5/2	3/2
		Ce ²⁹⁺	Cu I	9.067	1.4[14]	$3d^{10}4p$ 51% $(3d_{3/2}^9 4p_{3/2})_3 5f_{5/2}$	3/2	3/2
		Ce ²⁹⁺	Cu I	9.067	2.6[14]	$3d^{10}4d$ 33% $(3d_{3/2}^9 4d_{5/2})_2 5f_{5/2}$ + 34% $(3d_{3/2}^9 4d_{5/2})_3 5f_{5/2}$	5/2	7/2
2c	9.0797	Ce ²⁹⁺	Cu I	9.071	1.5[14]	$3d^{10}4d$ 63% $(3d_{3/2}^9 4d_{3/2})_2 5f_{5/2}$	3/2	5/2
		Ce ²⁹⁺	Cu I	9.072	1.4[14]	$3d^{10}4s$ 46% $(3d_{3/2}^9 4s)_1 5f_{5/2}$ + 44% $(3d_{3/2}^9 4s)_2 5f_{5/2}$	1/2	3/2
		Ce ²⁹⁺	Cu I	9.073	3.5[14]	$3d^{10}4f$ 35% $(3d_{3/2}^9 4f_{7/2})_3 5f_{5/2}$ + 28% $(3d_{3/2}^9 4f_{7/2})_4 5f_{5/2}$	7/2	3/2
2d	9.0888	Ce ²⁹⁺	Cu I	9.078	1.8[14]	$3d^{10}4f$ 67% $(3d_{3/2}^9 4f_{7/2})_5 5f_{5/2}$	7/2	5/2
		Ce ²⁹⁺	Cu I	9.081	1.7[14]	$3d^{10}4f$ 43% $(3d_{3/2}^9 4f_{7/2})_4 5f_{5/2}$ + 13% $(3d_{3/2}^9 4f_{7/2})_3 5f_{5/2}$	7/2	7/2
2e	9.0971	Ce ²⁹⁺	Cu I	9.084	1.5[14]	$3d^{10}4f$ 56% $(3d_{3/2}^9 4f_{5/2})_3 5f_{5/2}$	5/2	5/2
2f	9.1049	Ce ²⁹⁺	Cu I	9.099	2.7[13]	$3d^{10}4d$ 30% $(3d_{3/2}^9 4d_{3/2})_3 5f_{5/2}$ + 24% $(3d_{3/2}^9 4d_{3/2})_1 5f_{5/2}$	3/2	5/2
3	9.1271	Ce ³⁰⁺	Ni I	9.104	1.2[13]	$3s^2 3p^6 3d^{10}$ 100% $3s 3p^6 3d^{10} 4p_{1/2}$	0	1
4	9.1591	Ce ³¹⁺	Co I ^a	9.131	6.0[13]	$3p^6 3d^9$ 99% $(3p_{1/2}^5 3d_{5/2}^9)_2 4d_{3/2}$	5/2	7/2
5a	9.1884	Ce ²⁹⁺	Cu I	9.178	5.1[13]	$3d^{10}4f$ 27% $(3d_{5/2}^9 4f_{7/2})_1 5f_{5/2}$ + 12% $(3d_{3/2}^9 4f_{5/2})_1 5f_{5/2}$	5/2	7/2
5b	9.2045	Ce ²⁹⁺	Cu I	9.196	7.1[13]	$3d^{10}4p$ 20% $(3d_{5/2}^9 4p_{3/2})_1 5f_{7/2}$ + 38% $(3d_{5/2}^9 4p_{3/2})_3 5f_{7/2}$	3/2	5/2
5c	9.2106	Ce ²⁹⁺	Cu I	9.205	4.6[13]	$3d^{10}4p$ 62% $(3d_{5/2}^9 4p_{3/2})_3 5f_{7/2}$	3/2	3/2
5d	9.2172	Ce ²⁹⁺	Cu I	9.207	5.4[13]	$3d^{10}4s$ 55% $(3d_{5/2}^9 4s)_2 5f_{7/2}$	1/2	3/2
5e	9.2210	Ce ²⁹⁺	Cu I	9.211	5.5[13]	$3d^{10}4p$ 45% $(3d_{5/2}^9 4p_{1/2})_2 5f_{7/2}$ + 35% $(3d_{5/2}^9 4p_{1/2})_3 5f_{7/2}$	1/2	3/2
		Ce ²⁹⁺	Cu I	9.213	2.7[13]	$3d^{10}4s$ 82% $(3d_{5/2}^9 4s)_3 5f_{7/2}$	1/2	1/2
6a	9.2288	Ce ²⁸⁺	Zn I	9.233	1.6[14]	$3d^{10}4p_{3/2}^2$ 35% $[3d_{3/2}^9 (4p_{3/2}^2)_2]_{7/2} 5f_{5/2}$ + 28% $[3d_{3/2}^9 (4p_{3/2}^2)_2]_{5/2} 5f_{5/2}$	2	2
		Ce ²⁸⁺	Zn I	9.234	2.2[14]	$3d^{10}4p_{3/2}^2$ 27% $[3d_{3/2}^9 (4p_{3/2}^2)_2]_{5/2} 5f_{5/2}$ + 19% $[3d_{3/2}^9 (4p_{3/2}^2)_2]_{3/2} 5f_{5/2}$	2	3
6b	9.2407	Ce ²⁸⁺	Zn I	9.242	2.6[14]	$3d^{10}4s 4d_{5/2}$ 21% $[(3d_{3/2}^9 4s)_1 4d_{5/2}]_{5/2} 5f_{5/2}$ + 19% $[(3d_{3/2}^9 4s)_2 4d_{5/2}]_{7/2} 5f_{5/2}$	3	4
		Ce ²⁸⁺	Zn I	9.244	2.2[14]	$3d^{10}4s 4d_{5/2}$ 31% $[(3d_{3/2}^9 4s)_2 4d_{5/2}]_{7/2} 5f_{5/2}$ + 26% $[(3d_{3/2}^9 4s)_2 4d_{5/2}]_{9/2} 5f_{5/2}$	3	3
		Ce ²⁸⁺	Zn I	9.244	1.7[14]	$3d^{10}3s 4d_{3/2}$ 24% $[(3d_{3/2}^9 4s)_2 4d_{3/2}]_{5/2} 5f_{5/2}$ + 14% $[(3d_{3/2}^9 4s)_1 4d_{3/2}]_{3/2} 5f_{5/2}$	2	3
6c	9.2498	Ce ²⁸⁺	Zn I	9.252	3.2[14]	$3d^{10}4s 4f_{7/2}$ 20% $[(3d_{3/2}^9 4s)_1 4f_{7/2}]_{5/2} 5f_{5/2}$ + 18% $[(3d_{3/2}^9 4s)_1 4f_{7/2}]_{7/2} 5f_{5/2}$	4	5

^aTentative identification.

have been uniformly shifted by 9 and 2 mÅ, respectively. The two individual Ni-like lines and the Co-like line have been shifted by about 20 mÅ. It should be emphasized here that different configuration mixings are used for the calculations in each ionization state. Since the inclusion of different configuration mixings may change the values of the calculated wavelengths slightly (still within the uncertainty range of the calculations), no conclusion can be made here concerning the ionization dependence of the wavelength shift.

The shape of the lines in the experimental spectrum [upper trace in Fig. 2(a)], which results from the contributions of the physical line broadening, the spectrometer instrumental function, and the digitizing process of the exposed photographic film, appears to differ greatly from a Gaussian profile. It is found that the line shapes are better reproduced by assigning a Lorentzian profile in the simulated spectrum. Each line in the simulated spectrum is given a uniform width slightly smaller than the isolated experimental Ni-like line.

The best fitting of the synthetic spectrum with the experimental results is obtained when setting the electron density and temperature in the model to about 10^{22} cm^{-3} and 230 eV, respectively. The ionic population ratios for pairs of adjacent ionization states were estimated to be roughly $n_{\text{Ni I}}/n_{\text{Cu I}}=3$ and $n_{\text{Cu I}}/n_{\text{Zn I}}=1$. In the discussion that follows it is shown, however, that the accuracy of these ratios has no significant influence on the plasma diagnostic application under consideration. The comparison of the high-resolution experimental spectrum and the synthetic spectrum allows the identification of the resolved peaks. The identified peaks are labeled above the experimental trace in Fig. 2(a). Only the spectral features that were reproducible in several experimental spectra are labeled in the figure. In order to allow a clear distinction between groups of lines that belong to different transition arrays, the lines are labeled by a number and an additional letter; lines labeled with the same number belong to the same array (e.g., the lines labeled 2a to 2f all belong to the same transition array). The identification of the peaks is presented in Table I. The first column lists a label that identifies the line observed in Fig. 2(a). The Ni- and Co-like lines (labeled 1, 3, 4) were already identified in Ref. [4], but the present high-resolution spectrum allows for more accurate wavelength measurements. The next column displays the experimental wavelength λ_{exp} (Å). The following two columns give the emitting Ce ion and the isoelectronic sequence. The next columns display the computed wavelength λ_{theor} (Å), and the calculated Einstein coefficient (statistically weighted) for spontaneous emission, gA , for each line. The next column gives the detailed transition of the line (only the most important components of the eigenvector are given preceded by the square of their coefficients). The last two columns indicate the total angular momentum quantum number of the lower level, J_L , and of the upper level, J_U . The theoretical line wavelengths λ_{theor} (Å) given in the table are the values obtained prior to the minor shifts that were introduced for achieving the best fitting of the synthetic trace with the experimental spectrum in Fig. 2(a). It should be emphasized that in some cases the spectral distance between the partially resolved peaks within each array is beyond the accuracy limit of the theoretical calcula-

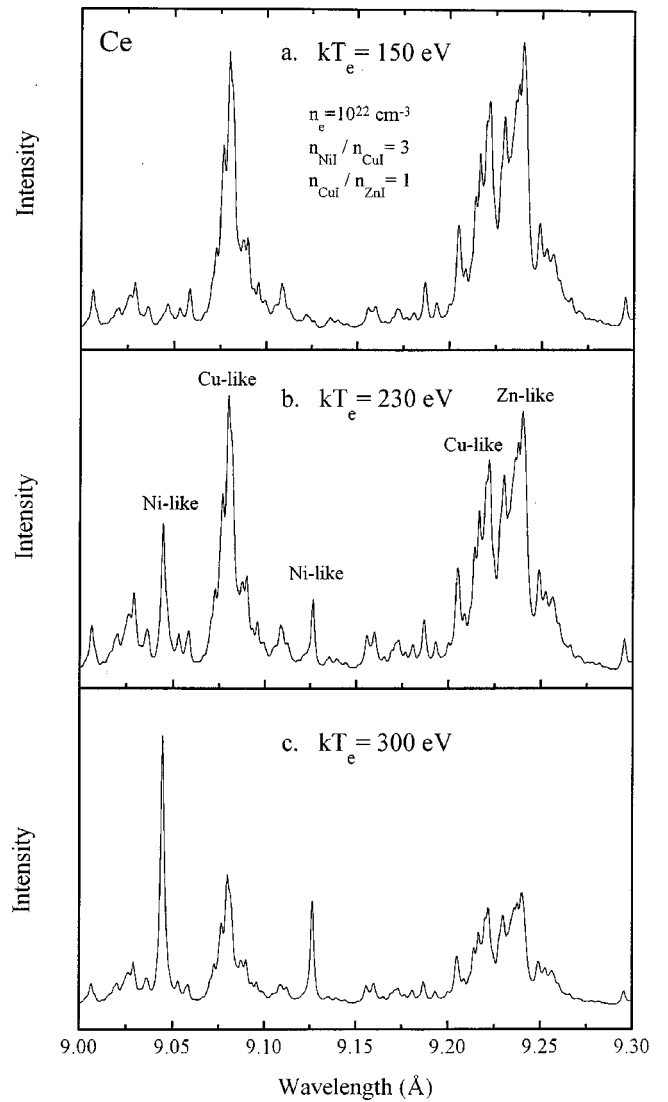


FIG. 3. Theoretical spectra of the 3d-5f Ni-, Cu-, and Zn-like Ce transitions (for the Ni-like ions the 3s-4p transition is also modeled) for three different electron temperatures: 150 (a), 230 (b), and 300 eV. (b) calculated for $n_e = 10^{22} \text{ cm}^{-3}$, $n_{\text{Ni I}}/n_{\text{Cu I}}=3$, and $n_{\text{Cu I}}/n_{\text{Zn I}}=1$.

tions. Therefore, while there is almost no doubt in the identification of the dominant transitions composing the UTA features, assigning the specific transitions to each of the partially resolved peaks may not be as definitive.

V. ELECTRON DENSITY AND TEMPERATURE ESTIMATE

The intensity ratio between the line arising from the Ni-like $3d^{10}-3d_{5/2}^9 5f_{7/2}$ resonant transition at 9.0450 Å and the transition array arising from the decay of the Cu-like $3d_{3/2}^9 n l 5f_{5/2}$ doubly excited levels in the range 9.06–9.10 Å is found to be very sensitive to the electron temperature T_e . This is clearly seen in Fig. 3, where synthetic spectra are plotted for different electron temperatures: 150, 230, and 300 eV, to be compared with the experimental spectrum [Fig. 2(a), thick trace]. The value of 230 eV gives the best fitting

between the synthetic and experimental spectra. At $kT_e = 150$ eV the intensity of the Ni-like resonant line is negligible compared to the Cu-like array, whereas at the relative high temperature of $kT_e = 300$ eV it becomes more intense than the Cu-like array.

The electron density is also estimated in the present work. From a comparison of the general aspect of the Cu-like high-resolution spectrum to synthetic spectra calculated for different densities, and from the intensity ratio between the $3p-4d$ and $3d-4f$ Ni-like lines, which are resolved in the low-resolution spectrum at 10.013 and 11.391 Å, respectively, one finds n_e to be in the range $(5 \times 10^{21}) - 10^{22}$ cm $^{-3}$. This range is similar to that found for the barium plasma ($n_e \sim 8 \times 10^{21}$ cm $^{-3}$) [7]. The electron temperature, estimated to be in the range 200–270 eV, however, is higher than that deduced for the barium plasma ($kT_e \sim 120$ eV). The fact that the energy of the laser pulse used in the present experiment (~ 25 mJ) is higher by about 20% than the energy used in the previous barium experiment cannot explain such a dramatic difference in the electron temperature. However, such a difference may be a consequence of the different types of transition used to diagnose the two plasmas. In the case of the barium plasma the electron temperature was deduced from the intensity ratios of lines arising from the decay of Cu-like autoionizing doubly excited levels only. The present cerium spectrum includes a Ni-like resonant line which arises solely from excitation processes, and Cu- and Zn-like arrays which can arise from either excitations or dielectronic capture (DC) processes. This allows an electron temperature estimate based on a comparison between excitation and dielectronic lines, which was not possible in the barium spectrum. It is important to note that an estimate of the electron temperature based solely on the intensity ratios of lines arising from the decay of doubly excited levels indicates a temperature lower than 230 eV in the present cerium plasma as well. However, due to the blending between the arrays belonging to the Cu- and Zn-like Ce ionization states [features labeled $5a-5e$ and $6a-6c$ in Fig. 2(a)], this analysis is inaccurate and therefore not presented here.

The present result deduced from the Ni- and Cu-like emission indicating a relatively high electron temperature can be understood by examining the T_e dependence of the main mechanisms for populating the relevant upper levels. In the electron density range of the present experiment the Cu-like $3d^9n15f$ configurations are populated mainly by two mechanisms: collisional excitations from lower Cu-like configurations and dielectronic capture processes from the Ni-like $3d^{10}$ ground or the $3d^94l$ singly excited configurations (at the electron density considered, three-body recombination is still much less important than DC). On the other hand, the $3d^9_{5/2}5f_{7/2}$ Ni-like level is mainly populated by only one mechanism: collisional excitations. Figure 4 presents the calculated mean rate coefficients of collisional excitation and dielectronic capture for the relevant transitions in Ni- and Cu-like cerium, as a function of T_e .

The mean rate coefficient $Q_{k'}^{\text{Ni I}}$ for collisional excitations into the $3d^9_{5/2}5f_{7/2}$ Ni-like level k' is weighted according to the populations of the lower Ni-like levels n_k obtained from

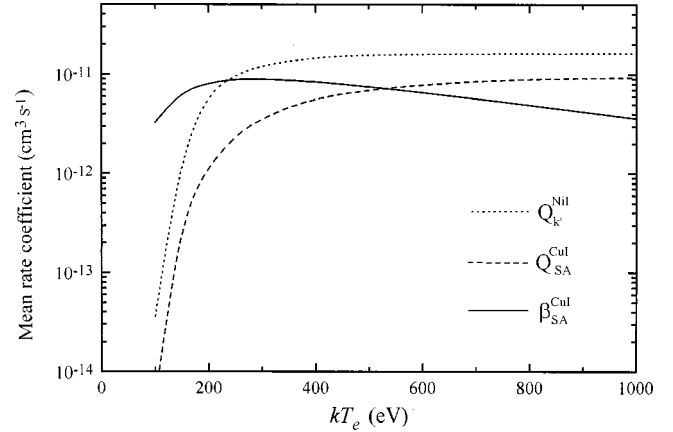


FIG. 4. Calculated mean population-weighted rate coefficients as a function of the electron temperature. $Q_{k'}^{\text{Ni I}}$ represents the mean rate coefficient for collisional excitation into the $3d^9_{5/2}5f_{7/2}$ Ni-like level. $\beta_{\text{SA}}^{\text{Cu I}}$ and $Q_{\text{SA}}^{\text{Cu I}}$ are the mean rate coefficients for dielectronic capture processes and collisional excitations, respectively, into the Cu-like doubly excited levels, which contribute to the subarray line transitions corresponding to the peak labeled $2c$ in Fig. 2(a).

the results of the first step of the collisional-radiative model, and is defined by

$$Q_{k'}^{\text{Ni I}} = \frac{\sum_{k < k'} n_k Q_{kk'}}{\sum_{k < k'} n_k}. \quad (2)$$

Analogous expressions are defined to describe the mean population-weighted rate coefficients for collisional excitations and for dielectronic captures responsible for populating the relevant Cu-like upper levels:

$$Q_{\text{SA}}^{\text{Cu I}} = \sum_{d \in \text{SA}} \frac{\sum_{i < d} n_i Q_{id}}{\sum_{i < d} n_i} \quad (3)$$

$$\text{and } \beta_{\text{SA}}^{\text{Cu I}} = \sum_{d \in \text{SA}} \frac{\sum_k n_k \beta_{kd}}{\sum_k n_k}, \quad (4)$$

respectively. The outer summations are performed over all of the doubly excited levels d that contribute to the emission of the Cu-like subarray (SA) line transitions. These transitions correspond to the main peak labeled $2c$ [Fig. 2(a)] as indicated in Table I. It can be seen from Fig. 4 that at relatively low electron temperatures, i.e., below 200 eV, the DC processes populating the Cu-like doubly excited levels are much stronger than the collisional excitations, both for the doubly excited Cu-like levels and for the $3d^9_{5/2}5f_{7/2}$ Ni-like level. Consequently, the intensity of the Ni-like resonant line,

which is mainly populated by collisional excitations, is negligible with respect to the Cu-like array [Fig. 3(a)]. As the temperature increases collisional excitations become important too. Since the mean rate coefficient for collisional excitation into the $3d^9_{5/2}5f_{7/2}$ Ni-like level is higher than the corresponding coefficient for the Cu-like subarray, the Ni-like line intensity is already comparable with the Cu-like array intensity at about 250 eV. The DC processes remain the dominant mechanism for populating the Cu-like doubly excited levels up to about 300 eV. In this DC-dominated regime the intensity of the Cu-like spectral features is approximately linearly dependent upon the population of the low Ni-like levels, as is the intensity of the Ni-like line; therefore, the accuracy of the ionic population ratio parameter $n_{\text{Ni I}}/n_{\text{Cu I}}$ is unimportant. In contrast, at relatively high electron temperatures, above 400 eV, when collisional excitations into the doubly excited levels ($Q_{\text{SA}}^{\text{Cu I}}$) become significant, the $n_{\text{Ni I}}/n_{\text{Cu I}}$ parameter plays an important role in determining the relative intensities of the Cu- and Ni-like emissions. In this case, one could obtain good agreement with the experimental spectrum also by setting the $n_{\text{Ni I}}/n_{\text{Cu I}}$ parameter to be much less than 1 (e.g., $n_{\text{Ni I}}/n_{\text{Cu I}} \sim 0.2$ at 500 eV). However, at these high temperatures the Ni-like ions are expected to be more abundant and such small values for the $n_{\text{Ni I}}/n_{\text{Cu I}}$ parameter are not consistent.

It is important to stress that the T_e deduced is based on a time- and space-integrated spectrum. In fact, one can assume that the Ni-like resonant line is mostly emitted from regions with somewhat higher temperatures than 230 eV, whereas the Cu-like dielectronic spectrum rather reflects regions with lower temperatures and particularly the cooling phase of the plasma [16]. Such a scenario is consistent with that described in the previous work on barium [7].

VI. CONCLUSIONS

The x-ray spectrum emitted by a highly stripped laser-produced cerium plasma has been recorded with a high-resolution curved mica crystal spectrometer in the limited range 9.0–9.3 Å and simultaneously with a flat RAP crystal spectrometer in a wider spectral range. The high-resolution spectrum was analyzed using a level-by-level collisional-radiative model which includes autoionization and dielectronic capture processes, and many lines or groups of lines have been identified. A comparison between the high-resolution experimental spectrum and synthetic spectra indicates an average electron temperature of about 230 eV, which is higher than the temperature deduced previously for a barium plasma in a similar experiment. This discrepancy can be explained by the fact that the barium plasma emission was interpreted using the relative intensities of lines emitted from Cu-like doubly excited levels only, whereas the present analysis is based on the intensity ratio of the satellite features emitted from doubly excited levels in Cu-like ions to the Ni-like resonant line, which mostly reflects a higher T_e region.

ACKNOWLEDGMENTS

E.B. was supported by the Charles Clore Israel Foundation. A.Y.F. and T.A.P. were supported in part by The Russian Fundamental Science Foundation, Grant No. 96-02-16111. This work was supported by the Hebrew University Intramural Research Fund Basic Project Awards.

-
- [1] D. Mitnik, P. Mandelbaum, J. L. Schwob, A. Bar-Shalom, J. Oreg, and W. H. Goldstein, *Phys. Rev. A* **50**, 4911 (1994).
 - [2] E. Behar, P. Mandelbaum, J. L. Schwob, A. Bar-Shalom, J. Oreg, and W. H. Goldstein, *Phys. Rev. A* **52**, 3770 (1995).
 - [3] M. Finkenthal, D. Stutman, and A. Bar-Shalom, *J. Appl. Phys.* **65**, 3786 (1989).
 - [4] R. Doron, E. Behar, M. Fraenkel, P. Mandelbaum, A. Zigler, J. L. Schwob, A. Ya Faenov, and T. A. Pikuz (unpublished).
 - [5] A. Zigler, P. Mandelbaum, J. L. Schwob, and D. Mitnik, *Phys. Scr.* **50**, 61 (1994).
 - [6] R. Doron, M. Fraenkel, P. Mandelbaum, A. Zigler, and J. L. Schwob, *Phys. Scr.* **58**, 19 (1998).
 - [7] R. Doron, E. Behar, M. Fraenkel, P. Mandelbaum, A. Zigler, J. L. Schwob, A. Ya Faenov, and T. A. Pikuz, *Phys. Rev. A* **58**, 1859 (1998).
 - [8] A. Ya. Faenov, S. A. Pikuz, A. I. Erko, B. A. Bryunetkin, V. M. Dyakin, G. V. Ivaneko, A. R. Mingleev, T. A. Pikuz, V. M. Romanova, and T. A. Shelkovenko, *Phys. Scr.* **50**, 333 (1994).
 - [9] G. Mourou, and D. Umstadter, *Phys. Fluids B* **4**, 2315 (1992).
 - [10] A. Ya. Faenov, B. A. Bryunetkin, V. M. Dyakin, T. A. Pikuz, I. Yu. Skobelev, S. A. Pikuz, J. Nilsen, A. L. Osterheld, and U. I. Safronova, *Phys. Rev. A* **52**, 3644 (1995).
 - [11] P. D. Rockett, C. R. Bird, C. J. Hailey, D. Sullivan, D. B. Brown, and P. Burkhalter, *Appl. Opt.* **24**, 2536 (1985).
 - [12] B. L. Henke and P. A. Jaanimagi, *Rev. Sci. Instrum.* **56**, 1537 (1985).
 - [13] R. Doron, E. Behar, P. Mandelbaum, J. L. Schwob, H. Fiedorowicz, A. Bartnik, R. Jarocki, M. Szczurek, and T. Wilhein, *Phys. Rev. A* **59**, 188 (1999).
 - [14] C. Breton and J. L. Schwob, *C. R. Hebd. Seances Acad. Sci.* **260**, 461 (1965); *ibid.* **261**, 1476 (1965); in *Some Aspects of VUV Radiation Physics*, edited by N. Damany, B. Vodar, and J. Romand (Pergamon, Oxford, 1974), pp. 250–256.
 - [15] A. Bar-Shalom, M. Klapisch, W. H. Goldstein, and J. Oreg, Computer Code HULLAC, 1988.
 - [16] W. Seka, J. L. Schwob, and C. Breton, *J. Appl. Phys.* **42**, 315 (1971).